

A novel approach to mapping ebb-tidal delta morphodynamics and stratigraphy

Stuart G. Pearson^{a,b,*}, Edwin P.L. Elias^b, Bram C. van Prooijen^a, Helena van der Vegt^b, Ad J. F. van der Spek^{b,c}, Zheng Bing Wang^{b,a}

^a Faculty of Civil Engineering and Geosciences, Delft University of Technology, P.O. Box 5048, 2600GA Delft, the Netherlands

^b Department of Applied Morphodynamics, Deltas, P.O. Box 177, 2600MH Delft, the Netherlands

^c Department of Physical Geography, Utrecht University, P.O. Box 80.115, 3508TC Utrecht, the Netherlands

ARTICLE INFO

Keywords:

Ebb-tidal delta
Ameland Inlet
Stratigraphy
Tidal inlet
Conformal mapping
Preservation potential
Morphodynamics

ABSTRACT

Ebb tidal deltas (ETDs) are highly dynamic features of sandy coastal systems, and coastal management concerns (e.g., nourishment and navigation) present a pressing need to better describe and quantify their evolution. Here we propose two techniques for leveraging the availability of high-resolution bathymetric surveys to generate new insights into the dynamics and preservation potential of ebb-tidal deltas. The first technique is conformal mapping to polar coordinates, using Ameland ebb-tidal delta in the Netherlands as a case study. Since the delta tends to evolve in a clockwise direction around the inlet, this approach provides an improved quantification and visualization of the morphodynamic behaviour as a timeseries. We clearly illustrate the sediment bypassing process and repeated rotational migration of channels and shoals across the inlet from updrift to downdrift coasts. Secondly, we generate a decadal scale (1975–2021) stratigraphic model from the differences between successive bathymetries. This stratigraphy showcases the delta's depositional behaviour through space and time, and provides a modern analogue for prehistoric ebb-tidal deltas. During the surveyed period, inlet fills form the largest and most stable deposits, while the downdrift swash platform is the most stable structure over longer periods. Together, these approaches provide new perspectives on ebb-tidal delta dynamics and preservation potential which are readily applicable to other sites with detailed bathymetric data. These findings are valuable at annual to decadal timescales for coastal management (e.g., for planning sand nourishments) and also at much longer timescales for interpreting stratigraphy in ancient rock records.

1. Introduction

Ceaselessly shaped, shifted, and shuffled around by the complex interaction of waves and tides, ebb-tidal deltas (ETDs) are dynamic morphological features whose behaviour affects navigation, coastal safety, and ecosystems. They form an essential, connected part of the regional sediment budget for tidal inlets, basins, estuaries, and barrier coasts (Rosati, 2005; Gelfenbaum and Kaminsky, 2010). Due to the large volumes of sand contained within them, ETDs are commonly viewed as a resource to be mined (Hicks and Hume, 1997; Fontolan et al., 2007). However, it has been recognized in the Netherlands that preserving ETDs (in part via sand nourishments) to maintain coastal sediment budgets is a potentially viable strategy for mitigating sea level rise and coastal erosion (Elias et al., 2012; Lodder and Slinger, 2021). Estimating the preservation potential of modern ETD and tidal inlet deposits is thus

essential for present-day coastal management. However, the possible fate of nourishments placed in such a dynamic environment is still largely unknown. The stochastic nature of meteorological forcing, highly nonlinear character of sediment transport, and complex morphodynamic feedbacks make predicting ebb-tidal delta evolution an ongoing challenge (Lenstra et al., 2019; Zhu et al., 2019). Mapping the evolution and preservation of ebb-tidal deltas and tidal inlets in order to better understand and predict their behaviour across multiple space and time scales is therefore a key research priority in coastal engineering and geoscience (Power et al., 2021).

Rising to meet such challenges demands new tools and techniques for interpreting ETD morphodynamics. This is difficult because it requires quantification and analysis of complex patterns in ever-changing bathymetry, which typically require numerical models, many measurements, and lengthy narrative descriptions to elucidate (Elias et al., 2019,

* Corresponding author at: Faculty of Civil Engineering and Geosciences, Delft University of Technology, P.O. Box 5048, 2600GA Delft, the Netherlands.
E-mail address: s.g.pearson@tudelft.nl (S.G. Pearson).

2022; Fortunato et al., 2021). Although the conceptual model of sediment bypassing around ebb-tidal deltas has been well-established for several decades (FitzGerald, 1983; Kana et al., 1999), the pathways that sediment takes across ebb-tidal deltas are still poorly understood (Son et al., 2011; Herring and Winter, 2018). We thus need techniques to distil the 4D (three spatial dimensions evolving through time) complexities of ETDs into more easily interpretable and comparable metrics and visualizations.

Just as we need new ways to characterize the dynamics of ETDs, we also need new approaches to quantify the sediment that remains deposited there. Early research on sediment preservation or stratigraphy in tidal inlets and ebb-tidal deltas was carried out principally in support of paleo-environmental reconstruction via modern analogues (Hubbard et al., 1979; Hayes, 1980; FitzGerald, 1984; Moslow and Tye, 1985; Imperato et al., 1988; Sha and De Boer, 1991; Tye and Moslow, 1993). In many of these cases, a key goal was to identify the potential for large sand deposits like tidal inlets and ebb-tidal deltas to be preserved as petroleum reservoirs. Sediment from ebb-tidal delta deposits typically survives in the ancient rock record as inlet channel fills (Mulhern et al., 2021). A perennial challenge in sedimentology is that preserved stratigraphy is discontinuous and seldom completely matches the initially-deposited stratigraphy due to distortion and “shredding” of the complete geological record by sediment transport (Jerolmack and Paola, 2010; Lazarus et al., 2019; Straub et al., 2020). A model of modern sedimentary preservation potential in ETDs would thus aid in the interpretation of the ancient rock record.

However, it is not just at geological timescales ($\mathcal{O}(10^6$ years)) that preservation potential is relevant. ETDs form key components of barrier coastal sediment budgets (Kaminsky et al., 2010; Elias et al., 2012; Oost et al., 2012), so understanding the nature of sediment preservation there on approximately decadal timescales ($\mathcal{O}(10^0 - 10^2$ years)) is essential for managing these coastal systems. What is the potential of ETDs to store sediment rather than bypassing it down the coast or importing it into the tidal basin? Which parts of the ETD are actively evolving on decadal timescales as opposed to remaining passively buried? Developing detailed stratigraphic models of modern ebb-tidal deltas may yield valuable scientific and coastal management insights into the nature of sediment storage there.

The age and preservation of ETD deposits can be estimated in numerous ways. Stratigraphy is preserved in the geological record and can be derived from cores or seismic data. However, such data (e.g., seismic surveys (Sha, 1989; Ronchi et al., 2019)) consider longer timescales of structural morphodynamic change caused by changing boundary conditions, and may not provide the temporal resolution required for coastal engineering and management. To achieve the necessary resolution, process-based numerical models can be used to develop synthetic stratigraphic models (Kleinhanus, 2010; Nicholas et al., 2016; van der Vegt et al., 2020). Alternatively, stratigraphic models can be constructed directly from repeated bathymetric surveys (Bridge, 1993; Sylvester et al., 2011), if they are sufficiently accurate and high in spatial and temporal resolution. Adopting a similar approach for ebb-tidal deltas would provide valuable insights into the sediment dynamics and preservation there.

Ameland ebb-tidal delta in the Netherlands has a long and rich history of bathymetric surveying, ranging from navigational charts made in the late 1500s to annual surveys in recent years (Elias et al., 2019, 2022). This dataset thus makes Ameland an ideal candidate for such an investigation of modern ETD architecture. In this paper, we present a novel analysis of high-resolution bathymetric surveys of Ameland ETD, constructing a decadal-scale stratigraphic model and projecting the bathymetry into polar coordinates that align with the dominant transport patterns. This technique can also be applied to bathymetric datasets computed by morphodynamic models. With this approach, we simplify the spatial and temporal complexity of ebb-tidal deltas and generate new perspectives on their dynamics and preservation.

2. Site background: Ameland ebb-tidal delta

Ameland Inlet lies between the barrier islands of Ameland and Terschelling in the northern part of the Netherlands (Fig. 1). On the North Sea side of the inlet, there is a large ebb-tidal delta characterized by a dynamic system of channels and shoals on its west side, and a more stable swash platform to the east. The surface of the ebb-tidal delta consists predominantly of well-sorted fine sand (mean $d_{50} = 211$ μm) with limited mud content (Rijkswaterstaat, 1999; Pearson et al., 2019). The 4 km-wide inlet connects the North Sea to the shallow Wadden Sea backbasin, and features a 30 m deep main channel (Borndiep) on the downdrift (east) side. On the updrift (west) side, the inlet consists of a shallow (approximately 5 m deep) platform that is intersected by smaller, highly dynamic channels.

The tide propagates along the coast of Terschelling and Ameland in an easterly direction, and is predominantly semi-diurnal. Ameland is a mixed-energy tidal inlet with a tidal range varying from 1.5 m at neap tide to 3 m at spring tide, and a tidal prism of $400 - 500 \times 10^6 \text{ m}^3$ (Elias et al., 2022). This tidal prism did not vary substantially between 1968 and 2017, and there has been no clear trend in residual ebb or flood dominance (Elias et al., 2022). Although other Dutch inlets have been dramatically changed in the past century by closure dams and other engineering works, Ameland has remained comparatively untouched during the 46-year period covered in this study. Although there are no major sources of fresh water within Ameland basin, episodic wind-driven flows lead to residual transport of fresh water from adjacent parts of the Wadden Sea into Ameland basin (Duran-Matute et al., 2016; Van Weerdenburg et al., 2021).

The North Sea in the vicinity of Ameland has a mild wave climate dominated by locally-generated wind waves. The mean significant wave height H_s at the adjacent island of Schiermonnikoog is 137 m (peak period T_p of 7.2 s), and H_s is less than 2 m for 83% of the time (Elias et al., 2022). Severe storms ($4.5 < H_s < 9.1$ m) occur less than 1% of the time, and generally take place in the winter months. Although the mean wind direction is from the southwest, the dominant wave direction is from the northwest. This wave climate drives a net eastward longshore sand transport estimated at between 0.3 and $1.2 \times 10^6 \text{ m}^3/\text{year}$ (Ridderinkhof et al., 2016; Elias et al., 2019).

3. Methodology & data

3.1. Polar analysis

To analyze the morphodynamic evolution of the ETD, we create a conformal map, an angle-preserving spatial transformation that allows complex geometries to be reprojected on a rectangular grid (Schinzing and Laura, 2003). Since the delta tends to evolve in a clockwise direction around the inlet (Elias et al., 2019), we plot the bathymetry in polar coordinates centred at the inlet. We can then stretch out the bathymetry and re-map it on a rectangular grid that is aligned with the main directions of shoal and channel migration. This approach enables the ebb-tidal delta's morphodynamic behaviour to be quantified more easily, since the grid can be further collapsed to a single spatial dimension. Although ETDs have often been simulated in process-based morphodynamic models along curvilinear and unstructured grids (Elias et al., 2006; Elkema et al., 2012) and radial coordinates have been used in some river delta models (e.g., Parker and Sequeiros (2006)), this type of gridding has not yet been used in this way to analyze decadal-scale bathymetry.

First, the origin and properties of the polar grid were selected. For Ameland Inlet, 607 km N, 169.5 km E (RD coordinate system) was chosen as the origin based on prior knowledge of the site's dynamics (Elias et al., 2019). This location is near the deepest part of the Borndiep, the main inlet channel, and remains stable throughout the surveyed period. A grid extent of 7 km from the origin was used because it lay within an area of consistent coverage area by the available bathymetric

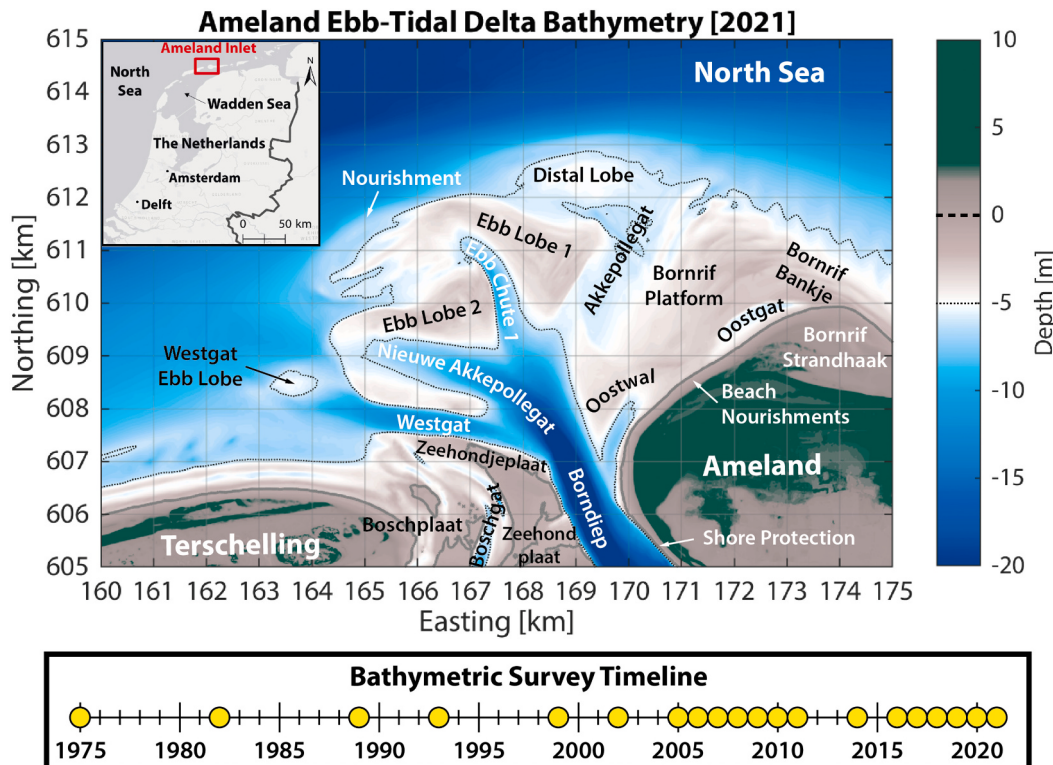


Fig. 1. Overview Ameland inlet and ebb tidal delta (circa 2021), located between the Dutch Wadden Islands of Terschelling and Ameland, in the north of the Netherlands. Key morphological features like channels and shoals are indicated, along with human interventions (e.g., nourishments and shore protection). Yellow dots on the timeline beneath the map indicate the years in which the bathymetry of the delta was surveyed. Bathymetry source: Rijkswaterstaat Vaklodingen. Elevation source: Actueel Hoogtebestand Nederland (AHN), Rijkswaterstaat. Basemap sources: Esri, HERE, Garmin, ©OpenStreetMap contributors, and the GIS user community. Translation of selected Dutch terms: “plaat” = shoal, “bankje” = (sand)bar, “gat” = channel or creek, “diep” = deep (channel), “strand” = beach, “haak” = hook, “nieuwe” = new, “oost” = east, “zeehond” = seal, “zeehondje” = baby seal. (For interpretation of the references to color in this figure legend, the reader is referred to the web version of this article.)

surveys. A 180°-wide swath from 260° (WSW) clockwise to 80° (ENE) was chosen as this extent was sufficient to capture the key morphodynamic processes of interest but excluded the inland portions of Terschelling and Ameland islands. Sensitivity testing revealed that the dominant bathymetric migration patterns coincided well with this origin and grid extent when compared with neighbouring alternative origins (see Supplementary Material). This step could be optimized in future applications to minimize distortions and constrain the validity of the method for a given inlet.

Next, the radial grid was overlaid on the raw bathymetric data. An angular resolution ($d\theta$) of 1° and radial grid spacing of 40 m were chosen, as this gave a good balance between having sufficient resolution in the coarser distal cells (approximately 40×120 m) and ensuring that there was at least one data point per cell in the proximal cells (approximately 40×20 m). To estimate the elevation of the polar grid cells (z_{polar}), all elevation points from the original rectangularly-gridded bathymetry (z_{rect}) lying within a given polar cell were averaged. Points within 1 km of the origin were neglected from the interpolation, since many of the polar grid cells within that radius were smaller than the 20 m resolution of the original bathymetric datasets.

To monitor volumetric changes in the delta through time, the sediment volume anomaly $V_{a(t)}$ within a given cell was calculated by multiplying its surface area A with the difference in elevation from the mean bathymetric surface z_{mean} . Since the interval between surveys was not equally spaced, each survey in the calculation of z_{mean} was weighted by the interval preceding it.

This procedure was repeated for all available surveys to create a three-dimensional timestamp of the delta's bathymetry. The evolution of the inlet can be further analyzed by collapsing the map along a single dimension, summing the volume anomalies $\sum V_{a(t)}$ along rows (ρ ,

distance from the inlet) or columns (θ , angular sector relative to 0° N). This permits the creation of Hovmöller (1949) or timestamp diagrams to illustrate the morphodynamics of the entire ETD in a single plot. This approach has been used at shorter timescales for specific regions of an ETD before (e.g., Harrison et al. (2017); Humberston et al. (2019)), but not yet for a whole delta or at decadal timescales.

3.2. Stratigraphy

To develop the stratigraphic model, we compare elevation (z) differences in the bathymetry at sequential timesteps t and $t + 1$ (e.g., Fig. 2). At all grid cells i where $z_{t+1,i} > z_{t,i}$, there is deposition and $z_{t+1,i}$ becomes the new surface elevation. The difference between $z_{t+1,i}$ and $z_{t,i}$ becomes labelled as a deposit with a date of $t + 1$, and $z_{t,i}$ remains the same for all previous values of t . At all grid cells i where $z_{t+1,i} < z_{t,i}$ there is erosion and $z_{t+1,i}$ becomes the new surface elevation. The elevation of z_t for all previous t is retroactively reset to $z_{t+1,i}$ and no deposition is recorded. This process is then repeated for all grid cells at all available timesteps.

The minimum bathymetric surface elevation across all surveys z_{min} defines the lower envelope of morphodynamic change during the total surveyed interval, which corresponds to the depth of reworking (e.g., van der Spek (1996); Vonhögen-Peeters et al. (2013)). Conversely, the maximum bathymetric surface elevation across all surveys z_{max} defines the upper envelope of morphodynamic change. The volume of sediment contained between z_{min} and z_t can be considered the “active” ETD (on the timescale of available surveys) V_{active} , while the volume of sediment beneath z_{min} can be considered the “passive” ETD ($V_{passive}$).

To estimate the age of a given surface deposit sample of depth Δz_{sample} , all deposit dates are first converted to an age from the most

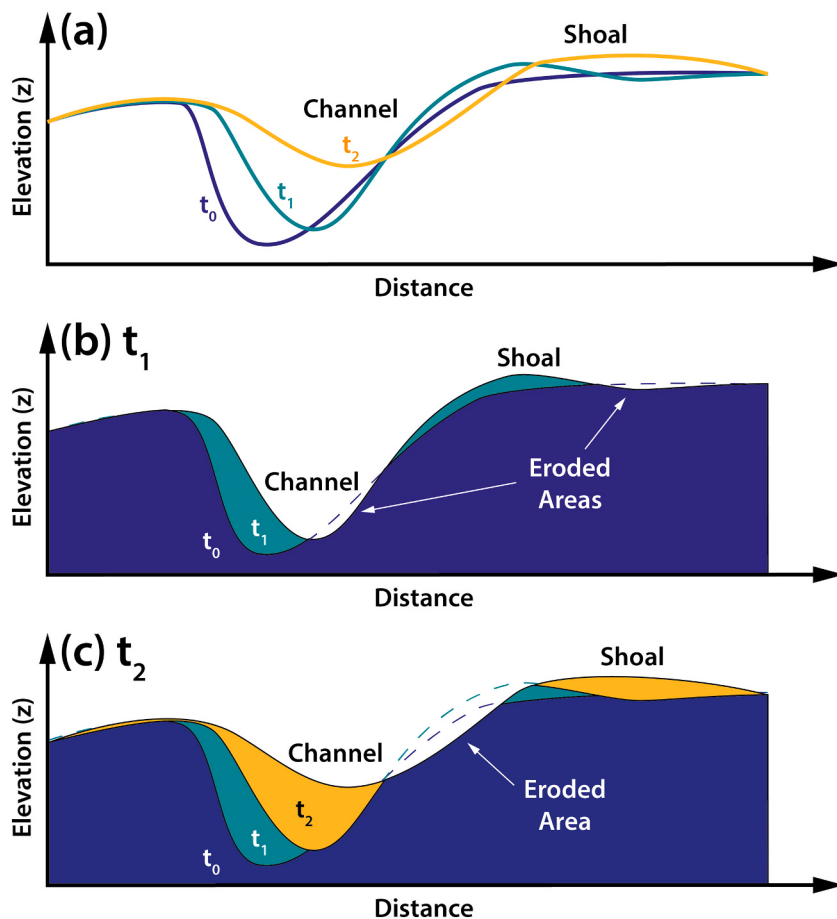


Fig. 2. Schematic diagram indicating how the stratigraphy is computed from (a) bathymetry at three sequential timesteps (t_0 , t_1 , t_2). For example, at t_1 (b), the channel migrates to the right and fills in slightly. The left part of the shoal accretes, but the right part erodes slightly below the t_0 elevation, z_0 . The areas deposited at t_1 are shaded in teal. At t_2 (c), the channel continues to infill and migrate to the right, eroding into t_0 and t_1 deposits. Sediment is also deposited on the shoal, as is indicated by yellow shading. This process is repeated for all grid cells in the bathymetry at all available timesteps. Note that eroded and deposited volumes are not necessarily conserved along the transect because it represents a 2D vertical slice of 3D stratigraphy. (For interpretation of the references to color in this figure legend, the reader is referred to the web version of this article.)

recent timestep. The mean deposit age across Δz_{sample} is estimated, weighted by the thickness of each deposit in the sample. This averaging is analogous to taking a surface core, but also reduces variability due to minor ($\mathcal{O}(0.1 \text{ m})$) differences in survey elevations. Note that this calculation reveals the time since the sediment was deposited, not the actual age of the sediment particles in that deposit. This approach does not explicitly consider the influence of sub-grid scale bedforms on sediment reworking. We also cannot say anything about grain size characteristics of the deposits, since we lack sediment size data in equivalent spatial and temporal resolution to the bathymetry.

3.3. Bathymetry

The two analysis techniques proposed here exploit the opportunities presented by high spatiotemporal resolution bathymetry. The earliest bathymetric surveys of Ameland Inlet were conducted for navigational purposes in the 1500s, and the area has been closely monitored in the centuries since then (Elias et al., 2019). These surveys were sporadic throughout the 20th century, but since 1989, Rijkswaterstaat (part of the Ministry of Infrastructure and Water Management) has measured the site at 3 to 6-year intervals and stored the data digitally as part of its *Vaklodingen* dataset (Fig. 1). In 2007–2010 and 2016–2021, more frequent surveys of the site (semi-annual to annual) were carried out as part of the SBW-Waddenzee and Kustgenese2.0 projects, respectively (Zijderveld and Peters, 2009; van Prooijen et al., 2020; van der Werf et al., 2019).

Subtidal areas of the study site were measured with a single-beam echo sounder in transects with approximately 200 m spacing. The data are reduced to 1 m resolution along transects after quality control is performed, after which the bathymetry is combined with nearshore

coastal profile measurements and LIDAR measurements of intertidal areas from the Dutch national elevation model, *Actueel Hoogtebestand Nederland* (AHN). The integrated digital elevation dataset is interpolated to a $20 \times 20 \text{ m}$ grid ($dx = 20 \text{ m}$), which forms the basis of the analysis presented here. Much more extensive descriptions of the Ameland Inlet bathymetric dataset used in the present study are given in Elias et al. (2019) and Elias et al. (2022).

4. Results

4.1. Bathymetry

Nearly 50 years of high-resolution bathymetric surveys are available for Ameland ETD, which provides a unique dataset that is well-suited to demonstrating our new analysis techniques. To characterize the delta, we first examine its average shape and its range of variability. The mean surface z_{mean} retains the key, persistent features of the ETD (e.g., Born-diep, Westgat, and Akkepollegat channels; Bornrif platform), but smooths out unique ephemeral features (Fig. 3a). This surface can thus serve as a basis of comparison for investigating the variability of ETD morphology.

The minimum bathymetric surface is dominated by the wide and deep Westgat and Born-diep channels (Fig. 3b). The western side of the delta is relatively deep ($< 6 \text{ m}$), since this region is repeatedly scoured down by migrating ebb-channels. Conversely, the Bornrif platform on the eastern side of the delta is relatively shallow and stable without intersections by deep channels.

The maximum bathymetric surface (Fig. 3c) has a fairly uniform elevation of approximately -3 m across much of the ebb-tidal delta. This depth is subtidal ($MLW \approx -1.4 \text{ m}$) but still well within the breaking

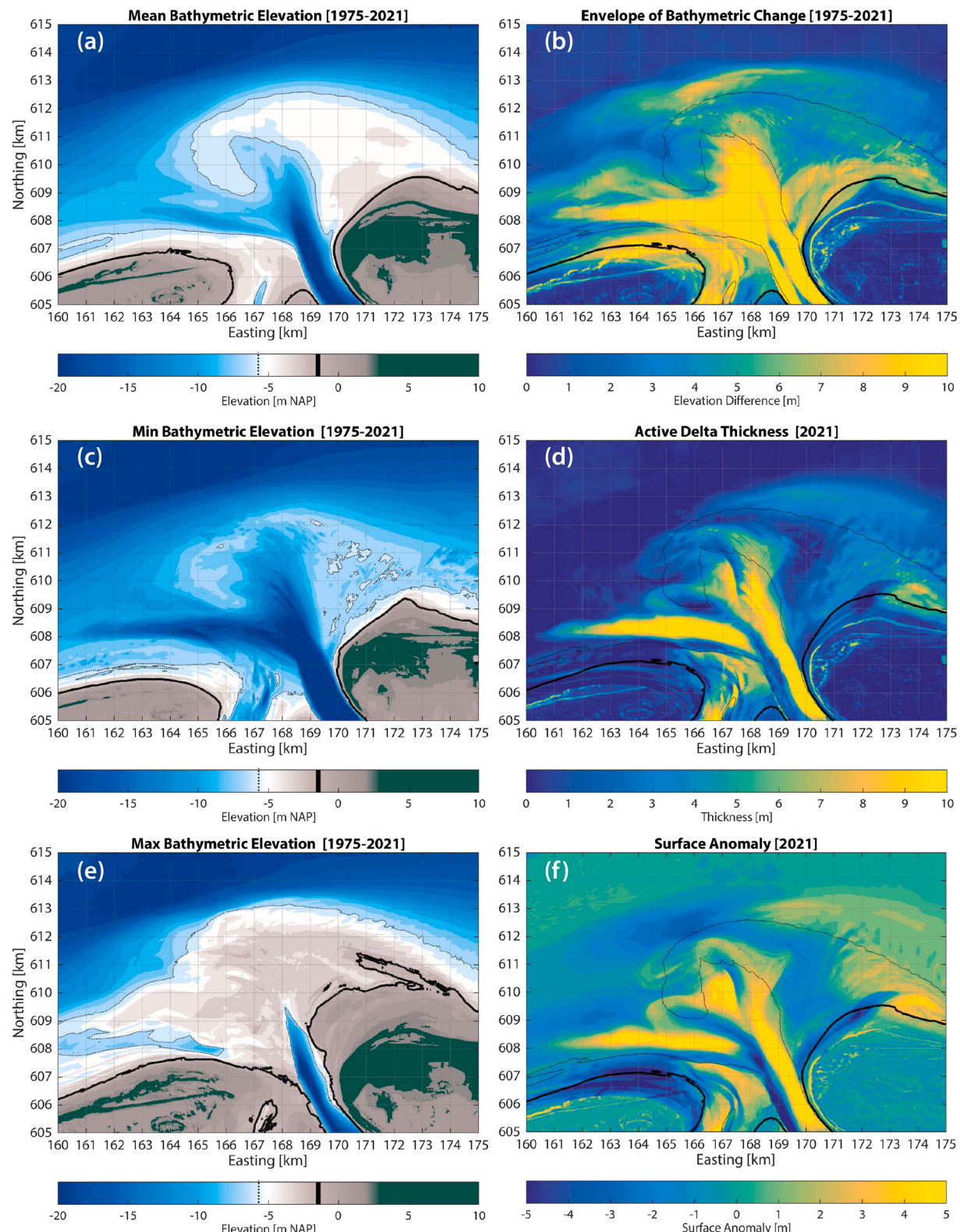


Fig. 3. Bathymetric surfaces derived from stratigraphic analysis. (a) Mean bathymetric elevation (z_{mean}). (b) Minimum bathymetric surface (z_{min}). (c) Maximum bathymetric surface (z_{max}). (d) The envelope of bathymetric change ($z_{max} - z_{min}$). (e) Active delta (preserved deposit) thickness in 2021 ($z_{2021} - z_{min}$). (f) Surface anomaly in 2021 ($z_{a, 2021} = z_{2021} - z_{mean}$). In (a, d, e, f), the approximate mean low water level (MLW) contour of the z_{mean} at -1.4 m NAP (Normaal Amsterdams Peil, approximately mean sea level) is represented with a thick black line, and the -6 m NAP depth contour is indicated with a thin dashed line. The MLW and -6 m contours in (b, c) correspond to those of z_{min} and z_{max} .

wave depth threshold for average wave conditions.

By computing the difference between the maximum and minimum bathymetric surfaces, we obtain the full envelope of observed morphological change (Fig. 3d). The envelope is thickest in the channel areas, but also on the Boschplaat where erosion of the island tip was substantial. The volume of the envelope between the maximum and minimum surfaces is given by:

$$V_{envelope} = \sum_{i=1}^n (z_{max,i} - z_{min,i}) \cdot dx^2 = 440 \times 10^6 \text{ m}^3 \quad (1)$$

where dx is the (fixed) rectangular grid cell width and n is the total number of rectangular grid cells within the boundaries of the polar grid defined in Fig. 4. The volume of sediment preserved in the active delta in 2021 is:

$$V_{active} = \sum_{i=1}^n (z_{2021,i} - z_{min,i}) \cdot dx^2 = 236 \times 10^6 \text{ m}^3 \quad (2)$$

This accounts for the volume of sediment that was deposited since 1975 and preserved in its original location until 2021 (Fig. 3e). Note that this is smaller than the volume of the envelope, indicating that the volume deposited and volume that is actually preserved differ by nearly a factor of 2. For comparison, Elias et al. (2022) computed the total net volume change $V_{net} = V_{2021} - V_{2005}$ and mean annual gross volume change $\bar{V}_{gross} = \bar{V}_{eroded} + \bar{V}_{deposited}$ of the delta from 2005 to 2021 as $18.3 \times 10^6 \text{ m}^3$ and $47 \times 10^6 \text{ m}^3/\text{year}$, respectively. These findings indicate that net changes in the size of the ETD are very small relative to the gross changes and that the morphodynamics of the delta are characterized by extensive reworking.

Lastly, we can compute the surface anomaly $z_{a(t)} = z_t - z_{mean}$ for each year, as indicated for 2021 in Fig. 3f. This corresponds to the height of the bed above or below the mean bathymetry, which makes it easier to monitor the migration of shoals and channels across the delta through time. In 2021, the most anomalous features are the shallower Borndiep and Westgat channels, massively eroded tip of the island Terschelling, twin ebb spillover lobes, nourishment, and Bornrif Bankje shoal.

4.2. Polar analysis

Plotting the ETD bathymetry in polar coordinates (Fig. 4a–f) aligns the grid with the principle sediment transport pathways (Pearson et al., 2020; Lambrechts, 2021): rotationally around the inlet (θ -axis), and radially out from the inlet (ρ -axis). The power of this conformal mapping approach arises when the complex geometry of the ETD (Elias et al., 2019, 2022) can be collapsed to a single spatial dimension. To do so, we compute the volume of sediment above and below the mean bathymetric surface (Fig. 3f). The computed volume anomaly $V_{a(t)} = z_{a(t)} \cdot dx^2$ is then summed across the θ and ρ directions for each surveyed year to produce a Hovmöller or timestamp diagram (Fig. 4g, h). In doing so, the essential morphological features of the ETD can be tracked in space and time.

Patterns in the volume anomaly with respect to θ correspond to rotational motion around the inlet (Fig. 4g). This makes it an ideal means of investigating sediment bypassing from one side of the inlet to the other via shoals. Bright yellow ridges indicate the presence of shoals, and dark blue troughs indicate channels or other deeper areas. These ridges and troughs show a clear trend up and to the right, which corresponds to a clockwise rotation of between 6 and $22^\circ/\text{decade}$. Cross-correlation analysis of the individual timesteps in Fig. 4g reveal that the entire delta rotates at an average rate of $11^\circ/\text{decade}$ from 1975 to 2021 (see Supplementary material for details). Several key patterns demonstrate this bypassing phenomenon (Fig. 4g):

- i. The persistent erosion of the Boschplaat at the tip of Terschelling ($\sim -90^\circ$), which began around 1975.

- ii. The infilling of the Westgat as its role changes from main ebb-channel to marginal flood channel.
- iii. A large volume of sediment migrates from the Boschplaat beginning in the 1990s, and gradually moves around the inlet to approximately -22.5° in 2021. This corresponds to the growth and migration of the Ebb Lobe 1 at $13.5^\circ/\text{decade}$ ($R^2 = 0.95$).
- iv. In 2005 at $\sim -55^\circ$, there is a bifurcation in this ridge, which corresponds to the outgrowth of Ebb Chute 2. The ebb delta nourishment in 2019 is visible as a small increase at the end of this ridge. The average migration rate of this shoal complex is $17.2^\circ/\text{decade}$ ($R^2 = 0.94$).
- v. The clockwise rotation of the Akkepollegat channel from 1989 to 2021 at $15.0^\circ/\text{decade}$ ($R^2 = 0.97$) and gradual infilling after 2015 as it loses its prominence as main ebb channel.
- vi. The migration of shoals across the Bornrif platform at $14.9^\circ/\text{decade}$ ($R^2 = 0.95$).
- vii. The migration of the proximal and distal parts of the marginal Oostgat channel at $10.1^\circ/\text{decade}$ ($R^2 = 0.88$) and $21.5^\circ/\text{decade}$ ($R^2 = 0.88$), respectively.
- viii. Attachment and migration of the Bornrif Strandhaak at $16.6^\circ/\text{decade}$ ($R^2 = 0.81$).
- ix. The gradual migration and attachment of the Bornrif Bankje shoal to the Ameland coast at $6.0^\circ/\text{decade}$ ($R^2 = 0.80$). The appearance of this shoal leads to an apparent bifurcation of the Oostgat channel (vii), although this is just an artefact of the chosen polar coordinate system.
- x. Erosion of the Ameland coastline associated with the westward migration and diffusion of the attached Bornrif Strandhaak shoal.

Patterns in the volume anomaly with respect to ρ correspond to expansion and contraction of the ETD in a radial direction from the inlet (Fig. 4h). We can divide the domain into three regions: proximal (1–3 km), medial (3–5 km), and distal (5–7 km). This behaviour is exemplified by these notable patterns:

- xi. The proximal region reflects the migration of a shoal complex from the tip of the Boschgat seawards, eventually becoming Ebb Lobe 1 and 2.
- xii. The medial region has a large volume anomaly in 1975 associated with the Bornrif shoal, which then attached to the Ameland coast and moved away from the inlet.
- xiii. The medial region increases in volume after 2010 due to seaward growth of Ebb Lobe 1 and 2 and attachment of Bornrif Bankje to the Ameland Coast
- xiv. The distal region has a large negative volume anomaly in 1975 because the Bornrif platform is then located further westward and closer to the inlet than in later years.
- xv. Prior to 1989, the distal region is dominated by the large volume of sand stored in the ebb lobe of the Westgat, which was then the main channel. Between 1989 and 2010, the distal region shows the landward contraction of the ETD associated with the migration of this mass of sediment from the distal lobe across the Bornrif.
- xvi. After 2010, the distal region grows seaward as Ebb Lobe 1 continues to develop and migrate around the periphery of the delta. The addition of the ebb delta nourishment in 2018 is also visible. This growth in the distal region also reflects the eastward migration of sediment from the Bornrif Bankje and Strandhaak after attaching to the Ameland coast.

Collectively, these patterns strongly suggest that sediment bypasses Ameland Inlet (at least in part) via shoals that migrate around the medial and distal region of the ETD. In the 46 years encompassed by the present study, no individual shoal makes a complete cycle across the entire inlet.

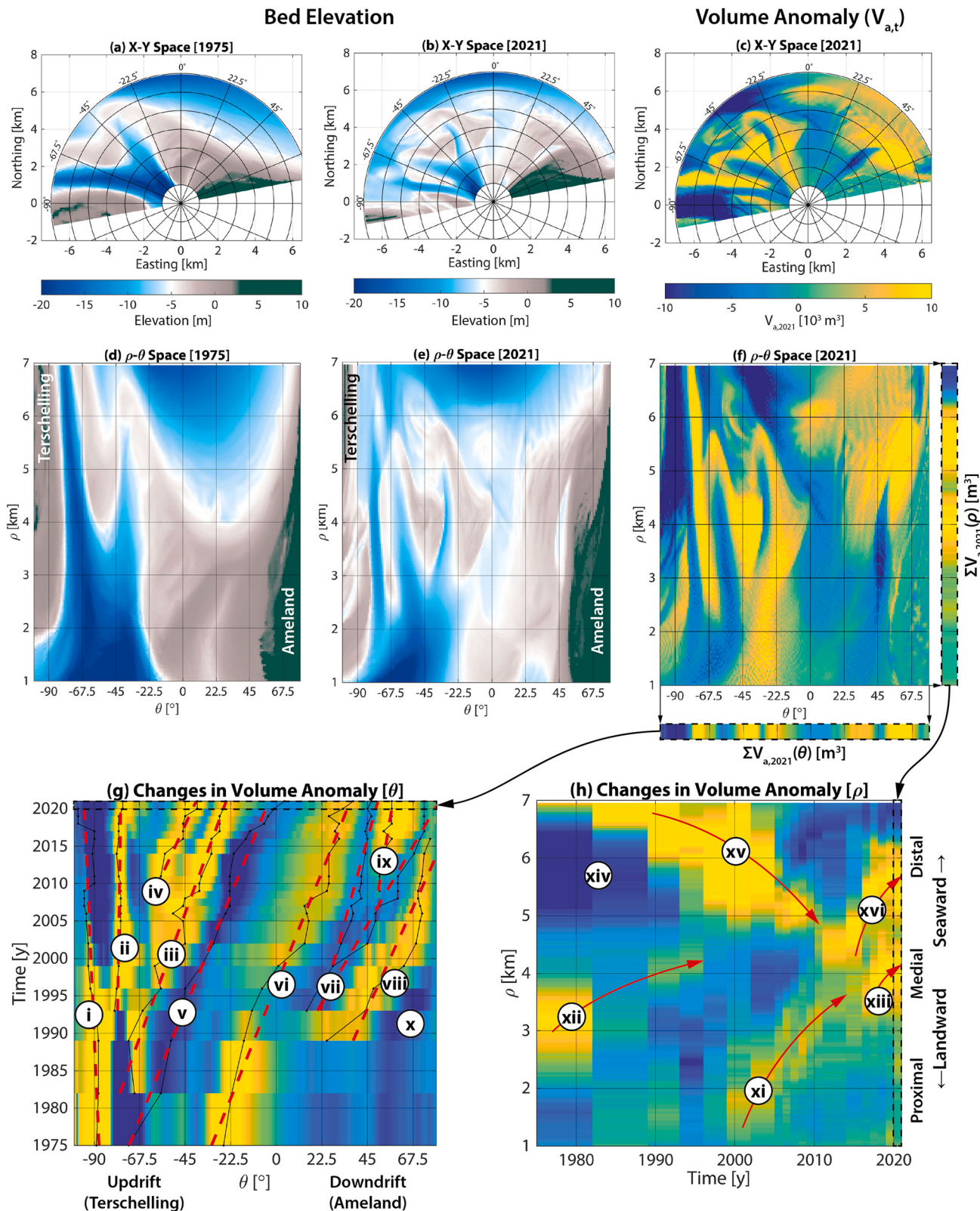


Fig. 4. Bathymetry of the ebb-tidal delta in Cartesian (top) and polar space (bottom) for the years 1975 (a, d) and 2021 (b, e). The volume anomaly $V_{a(t)}$ (volume of sediment in a given year (here 2021) above or below the mean bathymetric surface z_{mean}) is given in Cartesian (c) and polar space (f). Hovmöller diagrams indicate the change in volume anomaly for each year summed along the θ (g) and ρ axes (h), stacked in time. For example, the sum of each column in (f) is the top row of (g), and the sum of each row in (f) is the right-most column of (h). In (g), thin black lines denote the trajectory of shoals or depositional areas (yellow) and channels or eroded areas (blue) in space and time. Red dashed lines indicate linear fits through those trajectories. Trends up and to the right in $\theta - t$ space (g) indicate clockwise motion around the inlet. Trends up and to the right in $\rho - t$ space (h) indicate seaward expansion of the delta, and are qualitatively shown by red arrows. (For interpretation of the references to color in this figure legend, the reader is referred to the web version of this article.)

4.3. Stratigraphic model

To explore the stratigraphic model, we examine seven vertical cross-sections through the ebb-tidal delta (Fig. 5), chosen to best illustrate key morphodynamic behaviours:

- **Section A-A'** spans the width of the inlet between the islands of Terschelling and Ameland. The Boschplaat (the eastern tip of the island Terschelling, $X = 2 - 5$ km) eroded nearly 3 km westward in the past 50 years (Elias et al., 2019). The shoal and channel complex left behind in its wake at the centre of the inlet ($X = 3 - 6$ km) is highly dynamic. From $X = 2 - 4$ km, the active depth reaches around -4 m, whereas eastward ($X = 4 - 6$ km) the active layer extends deeper to about -6 to -10 m. This is a result of the dynamic secondary channels that continuously rework the sediment. Even though Zeehondjeplaat ($X = 5 - 6$ km) retains its height, the deposit age indicates that it has been heavily reworked (to a considerable depth – down to -10 m). This apparently stable shoal is actually highly morphodynamic.

There is a clear channel fill sequence as the main ebb-channel (Borndiep) migrates westward at this location ($X = 6 - 7$ km). Note, however, that south of this transect, the channel migrates eastward into the island, necessitating shore protection works and nourishments.

- **Section O-B'** extends northwest from the inlet across the Kofmansbult platform. There are extensive channel fills in the proximal part of the Borndiep (1-2 km), but the distal parts of the profile are characterized by extensive recent deposition in subtidal ebb spillover lobes. The seaward growth of these lobes is evident from the steep lee slopes of progressively newer deposits (at ~ 4 km), whereas the rear slope (at 1.5–3.5 km) is much milder and eroding into older deposits. The active deposits in this transect are typically 4–8 m thick, since this cross-section roughly follows the former centreline of the Akkepollegat ebb channel. The maximum shoal height appears to decrease with distance, from -2 m between 2 and 3 km to almost -4 m at 6–7 km. In 2018, a 5×10^6 m³ sand nourishment was placed at the seaward edge of the profile (6–7 km).
- **Section O-C'** extends due north of the inlet through the Akkepollegat ebb channel. At the proximal end of the section there are deep deposits associated with infilling of the Borndiep (0–2 km) and the growth of the Oostwal shoal. Recent deposits in the middle of the section are thin or non-existent, as in 2019 the Akkepollegat is migrating laterally and eroding into older sediment (2–5 km). At the far end of the transect lies the distal lobe deposits of the delta (5–7 km).
- **Section O-D'** cuts northeast past the tip of Ameland and across the Borndiep swash platform. In 2019, the beach of Ameland was nourished (0.5–2 km) to limit coastal erosion there. This nourishment filled in part of a shallow marginal channel, the Oostgat, which persists in the middle of the transect (2.5–4.5 km). The channel has been gradually squeezed against the Ameland coast, so there is relatively little deposition there. At the distal end of the profile lies the Bornrif Bankje, a large sandy shoal that began attaching to the Ameland coast in about 2016 (Elias et al., 2019).

A crucial difference between the Oostgat and the main channels to the west (i.e., Borndiep, Westgat, and Akkepollegat before 2011) is that it does not scour beneath the surface of the Bornrif platform. Its definition as a channel is mainly due to the development of shoals on either side of it (see also Section F-F').

- **Section E-E'** is a 6 km long arc spanning the proximal part of the delta at a radius of 2 km from the origin. Recent shallow channel fills at 0–1 km are associated with shoal development at the tip of the Zeehondjeplaat. The much older and deeper channel fills between 0.8 and 1.5 km are connected with the infilling of the Westgat, which used to be the primary ebb channel from the 1950s–1980s (Elias et al., 2019). Channel fill between 1.5 and 3 km corresponds to the

switch of the main ebb-channel from the Westgat to the Akkepollegat, beginning in the 1980s. The Akkepollegat migrated laterally with a fairly persistent base of -19 m until approximately 2007, at which point it began to diminish in importance and accrete vertically. In contrast to the steeper-banked active channels (e.g., A-A' at 7 km), infilling channels on the ETD tend to have more gradual side slopes, and are deposited in much thinner layers (e.g., at 2.5 km). At 3–5 km, the gradual progradation of the Oostwal shoal can be seen. At 5 km, the 2019 beach nourishment fronts the Ameland coast, on which high dunes extend above the intertidal zone.

- **Section F-F'** cuts across the medial part of the delta (4 km from the origin) and spans from the Boschplaat to Ameland, clearly demonstrating the shoal bypassing process illustrated in Fig. 4. Between 1 and 3 km, the extensive channel fill of Westgat seen in Section E-E' continues. Westgat has continued to narrow in recent years as the Nieuwe Akkepollegat channel (2–3 km) widened and encroached southward (~ 2 km). Ebb Lobe 2 emerged at the tip of Nieuwe Akkepollegat, outbuilding laterally on both sides and migrating clockwise around the inlet, encroaching on Ebb Chute 1. Ebb Chute 1 and Ebb Lobe 1 are migrating clockwise and encroaching on Akkepollegat, the former main ebb channel. This migration tends to occur most rapidly during fall and winter storms (Elias et al., 2022). Vividly illustrating this process, a measurement frame placed at 168.46 km N, 610.44 km E (53.48° N 5.59° E) on September 19, 2017 was irretrievably buried beneath the migrating Ebb Lobe 1 during a large northwesterly storm on October 3–7, 2017.

The minimum surface along F-F' between approximately 4–8 km corresponds to the former and current base of the Akkepollegat channel and Ebb Chute 1. Section F-F' shows the fate of a former main ebb channel – as Akkepollegat migrated eastward, more and more flow was diverted to the western channels (Elias et al., 2019). Akkepollegat still scours the main platform, but only a shallow channel forms – it does not have the strength to carve a pronounced channel here (see also O-C'). The western channel embankment only forms as Ebb Lobe 1 pushes eastward.

On the eastern bank of the Akkepollegat, a shallow shoal steadily accretes vertically and migrates shoreward across the Bornrif platform, encroaching on the Oostgat marginal channel (2–3 km). The maximum surface elevation reveals that the ETD at this radius from the inlet has remained completely subtidal, at an average depth of 3 m. At the coastline (11 km), the remnants of the Bornrif Strandhaak (a shoal which attached to Ameland in the 1990s) are visible, although it has been eroded and subsequently re-deposited by the Oostgat.

- **Section G-G'** spans a 17 km transect along the distal end of the delta, 6 km from the origin. The shoreline of Terschelling has retreated by over 1 km, encroached by Westgat (0–2 km). Between 2 and 3 km, the vertical infilling of the formerly-dominant Westgat is evident, and this area is now capped by an ebb-tidal shoal at the end of the present-day channel. The 2018 ETD nourishment sits between 4 and 7 km atop the seaward edge of Ebb Lobe 1. The relatively recent distal lobe spans from 7 to 12 km, and migrates in a clockwise (locally, eastward) direction. The eastern edge of the delta (12–17 km) is characterized by a series of onshore-migrating sawtooth bars, discussed in greater detail by Brakenhoff et al. (2019). At the Ameland coast, the more recent Bornrif Bankje (circa 2015) abuts against the older deposits of the Bornrif Strandhaak (circa 1989).

The stratigraphic model provides an additional perspective on the ebb-tidal delta dynamics revealed by the polar analysis. The arc transects of E-E', F-F', and G-G' depict the same clockwise migration patterns demonstrated in Fig. 4g. Similarly, the radial transects O-B', O-C', and O-D' indicate sedimentary structures that correspond to the seaward growth of the delta observed in recent years (Fig. 4h).

In addition to the delta's dynamic behaviour, the stratigraphic model shows much about the less mobile sedimentary deposits that remain

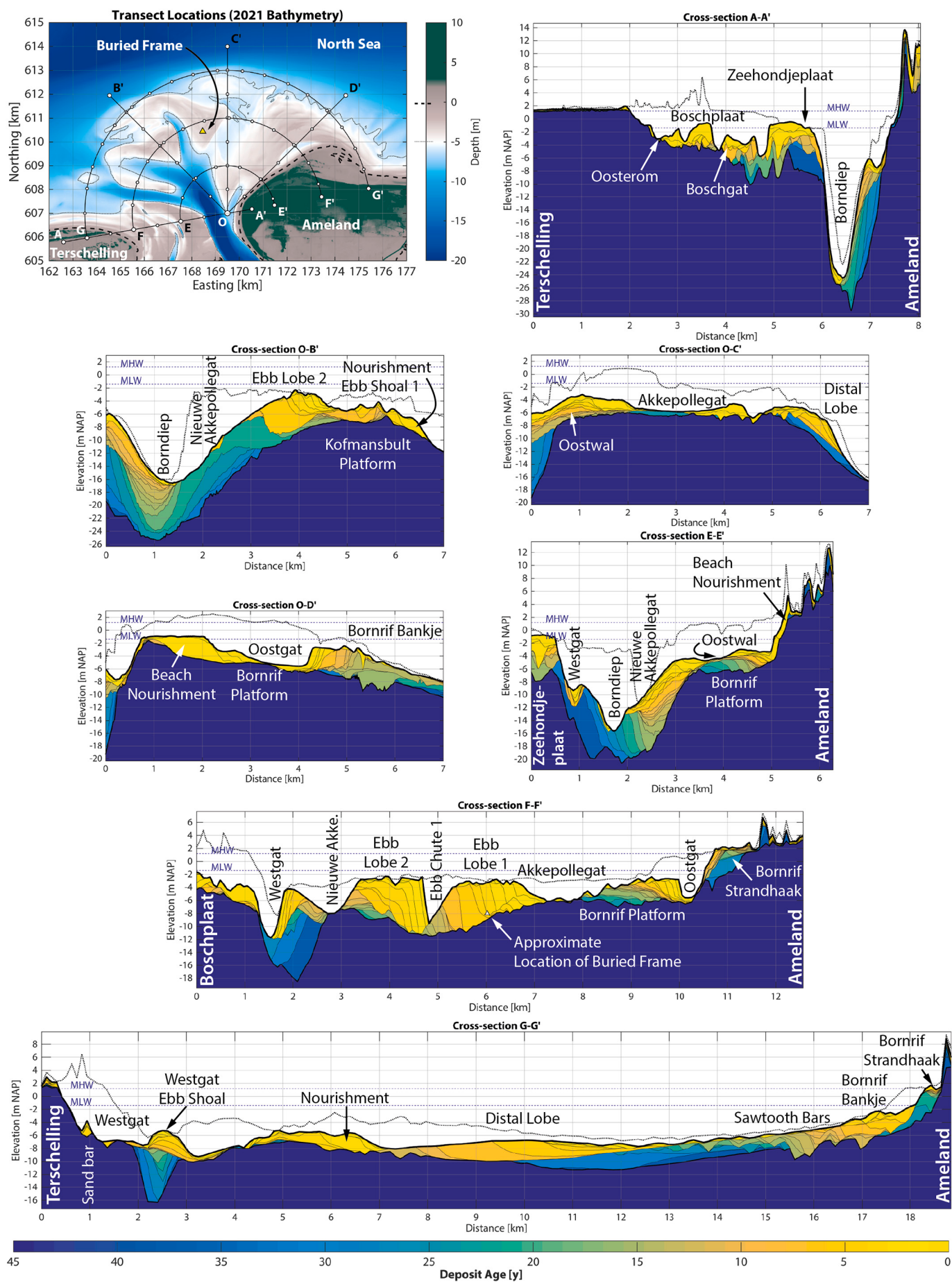


Fig. 5. Ameland ebb-tidal delta bathymetry and stratigraphic sections. The maximum surface elevation across all surveys is given by a thick dotted line. Mean Low Water (MLW, -1.4 m NAP) and Mean High Water (MHW, $+1.2$ m NAP) are indicated with blue dotted lines. Small white circles on the transect location map correspond to the 1 km intervals on the x-axes of the accompanying cross-sections. See Fig. 2 for an explanation of how to interpret the transects. The small triangle in the map and F-F' represents the approximate location of a measurement frame that was buried beneath the migrating Ebb Lobe 1 during a storm in October 2017. (For interpretation of the references to color in this figure legend, the reader is referred to the web version of this article.)

preserved. The surface deposits of Ameland ebb tidal delta circa 2019 are generally young (<5 years), which reflects the continuous reworking of the system (Fig. 6).

The oldest areas of exposed sediment correspond to channel incision and migration in Ebb Chute 2, Westgat, the seaward tip of Akkelpollegat, and Oostgat. Older material is exposed on the shoreface west of the delta, whereas the shoreface east of the delta is more freshly deposited. Bar migration on the upper shoreface of Terschelling reveals alternating patterns of older and younger sediment.

Beneath the present-day surface, large portions of the ebb-tidal delta have remained undisturbed for at least the last 46 years. These are indicated by the oldest, dark blue sediment in Fig. 5 and the shallowest regions of the minimum bathymetric surface in Fig. 3b. The most stable parts of the ebb-tidal delta appear to be the Bornrif platform to the east and the deeper parts of the Kofmansbult platform to the west. The majority of shoals on the ETD are continuously reworked on timescales of less than 10 years.

5. Discussion

In this study, we developed a combination of techniques for mapping and analyzing the decadal scale morphodynamics and stratigraphy of a mixed-energy ebb-tidal delta. This approach leverages bathymetric data in ways that provide new insights into the dynamics of present-day ETDs or the strata left behind by ancient ETDs. The conformal mapping (polar) analysis collapses large amounts of spatiotemporal bathymetric data into a single figure that clearly shows key morphodynamic behaviour like ebb-tidal delta bypassing. The combination of conformal mapping and stratigraphic modelling provides greater interpretive value than either approach in isolation. Our approach also gives useful information for dealing with contemporary coastal management issues like nourishment planning, by indicating where deposited sediment is more likely to migrate or persist. This methodology is generally applicable to any coastal or submarine landscape where high resolution (in space and

time) digital elevation models or numerical model output are available. We demonstrated this technique by applying it to 46 years of bathymetric surveys from Ameland ebb-tidal delta in the Netherlands. Together with the narrative explanation of morphological evolution from studies like Elias et al. (2019, 2022), these techniques provide a powerful set of tools for analyzing and interpreting ebb-tidal delta dynamics.

5.1. Preservation potential

The stratigraphic model developed here provides insight into the preservation potential of Ameland ebb-tidal delta on yearly and decadal timescales. Deposits are eroded rapidly at first, and then more gradually after several years. Surficial sediments are extensively reworked, indicative of the large gross but small net changes observed there (Elias et al., 2022). The thickest deposits with the greatest preservation potential over the observed timescale are channel fills (Figs. 5 and 3e). With the exception of some deeper channel fills, the majority of sediment deposited in the 1970s to 1990s has already been reworked by the 2021 (Fig. 5).

Via this approach, we can clearly demarcate the active and passive parts of the ebb-tidal delta on decadal timescales. The passive (blue) part and the ebb-tidal delta as a whole are governed largely by the tidal prism (Walton and Adams, 1976). Conversely, we hypothesize that the active (yellow) part fluctuates in response to the sediment bypassing process. This distinction is particularly useful in the case of features that appear relatively stable but are in fact continuously reworked (e.g., Zeehondjeplaat in Fig. 5 Section A-A').

Our analysis does not consider regions which are stable over much longer periods than the 46 years analyzed here. Elias et al. (2019) indicate that the Bornrif platform has been very stable for the past two centuries with no major channel bisections since 1831, when a channel extended northeast across it to depths greater than 7 m. The Bornrif is a remarkably persistent feature, present in its familiar form as far back as

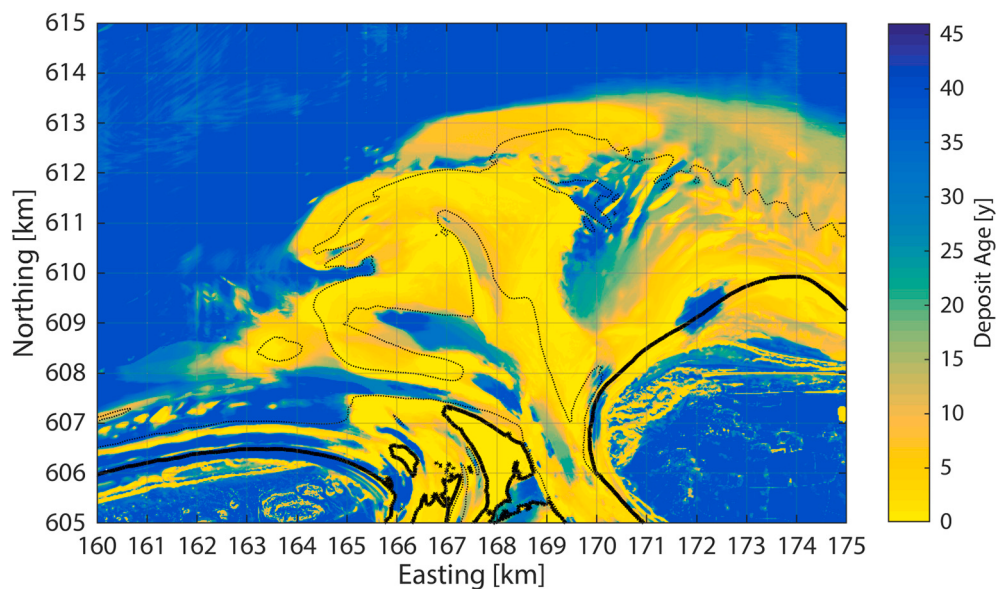


Fig. 6. Surface deposit age, calculated using the average age of deposits in the top 1.0 m of the seabed. The approximate mean low water level (MLW) contour at -1.4 m NAP (*Normaal Amsterdams Peil*, approximately mean sea level) in 2021 is represented with a thick black line, and the -6 m NAP depth contour is indicated with a thin dashed line.

the first available nautical charts in 1585. Conversely, the main ebb-channel nearly always occupies the northwest quadrant of the delta, and although deposits there tend to be thick, this area is subject to frequent reworking. Ages of preserved deposits derived using our method could be further verified in the field with geochronological methods (e.g., Reimann et al. (2015); Fruergaard et al. (2015)).

5.2. Sediment dynamics

Sediment bypassing across the delta in shoals can now be more accurately quantified with the techniques shown here. The clockwise migration of shoals and channels around the inlet is corroborated by both the polar analysis and stratigraphic model (e.g., Fig. 4g and Cross Section F-F' of Fig. 5). Although this is perhaps unsurprising given that their underlying datasets are the same, it demonstrates their combined usefulness for interpretation of complex patterns.

The utility of the polar/conformal mapping approach extends to sediment properties like grain size. Projecting sediment samples from Ameland ebb-tidal delta into polar coordinates illuminates a clear decreasing trend and reduction of variability in median grain size (d_{50}) clockwise around the inlet (Elias et al., 2022). This coincides with the direction of shoal migration and channel rotation mapped in Fig. 4g. van der Vegt (2018) also demonstrated spatial variation in grain size of river deltas using polar mapping.

It is not possible to conclusively estimate the duration of a full bypassing sequence from the present data, since the longest continuous ridges or troughs in Fig. 4g traverse no more than halfway around the inlet. Previous estimates of Ameland's bypassing period estimated a cycle duration of 50 to 60 years (Israel and Dunsbergen, 1999; Ridderinkhof et al., 2016; Cheung et al., 2007). The timescale of main ebb channel switching appears to be on the order of 50 years, given that the primary ebb channel (Nieuwe Akkепollegrat) in 2021 is west-aligned for the first time since 1975. Elias et al. (2019) suggest that multiple small bypassing events may be necessary to create sufficient shoal volume on the downdrift platform to trigger a major shoal bypassing event.

The results of Fig. 4g make it apparent that the definition of a bypassing cycle needs clarification: is it just the time between shoal attachments on the downdrift coast, or is it about tracking a discrete plug of sand from one side of the inlet to the other? Multiple forms of shoal bypassing can exist, with differently-sized shoals migrating along different pathways and at varying timescales. These shoal migrations may be due to the migration of the main ebb channel (e.g., on the Bornrif Fig. 4g (v)) or may arise from local instabilities (e.g., the initial formation of ebb chutes Fig. 4g (iii)). We hence advocate for using the term bypassing “sequence” (as per Elias et al. (2012)) in lieu of “cycle” to better reflect the often nonlinear, discontinuous, and aperiodic nature of the process.

Furthermore, bar migration is not completely representative of the sediment bypassing process since part of the transport is in suspension. A recent tracer study at the Ameland ETD nourishment site indicated that individual grains of sand can migrate several kilometers in just a few tidal cycles (Pearson et al., 2021b), which is more indicative of gross transports than the net transport represented by shoal migration. The adoption of Lagrangian sediment transport models (e.g., MacDonald and Davies (2007); Soulsby et al. (2011); Pearson et al. (2021a)) could be used to identify the transport pathways connecting eroding and depositional regions of the ETD.

5.3. Coastal management implications

Coastal management and policy makers require new tools and approaches in order to make informed decisions (Lodder and Slinger, 2021). Our new mapping approaches show the storage potential of ETDs for sediment on annual to decadal timescales. Understanding the changes in the active volume of the ETD may lead to better estimates of when it is acting as a net sediment source or sink. This knowledge can

inform nourishment strategies by indicating where and when to nourish, depending on the location and longevity of existing deposits. Placing a nourishment in an (comparatively) inactive zone will lead to less dispersive behaviour than placing it a highly dynamic zone. The choice depends on the goal of the nourishment (preserving volume versus increasing sand fluxes in a specific location).

For instance, the clockwise migration of shoals at approximately 10–15°/decade (Fig. 4g) suggests that the bulk of the nourishment placed in 2018 will likely take several decades before reaching the downdrift Ameland coast. If the goal is to directly feed Ameland, it should be placed closer to the shore (e.g., at the location of the beach nourishment in Fig. 5 Section E-E'). However, for a goal of increasing the total sediment budget of the ebb-delta on longer timescales, the location of the 2018 nourishment was likely a good choice.

Equilibrium models are frequently used to predict the evolution of ETDs at timescales of 10 to 100+ years (Stive and Wang, 2003; Lodder et al., 2019; Wang et al., 2020). These models typically schematize ETDs as homogeneous deposits that directly exchange sediment with neighbouring coasts and basins. Recent numerical modelling studies (Herrling and Winter, 2018; Pearson et al., 2020) reveal complex sediment pathways across ETDs and their surroundings, which are also reflected by the patchiness of sediment deposition presented here (Fig. 5). This calls into question the assumption of perfect, symmetric sediment connectivity between the ebb-tidal delta and other components of the coastal system. Understanding the actual spatial heterogeneity of ETD deposits and the resulting implications for sediment connectivity is essential to making good long-term predictions of these systems.

In addition to planning nourishments, understanding where stable and unstable areas of ETDs are located is important for protecting coastal and submarine infrastructure (e.g., cables and pipelines), as eroding coasts and nearshore regions pose hazards for these (Eide et al., 1992; Pearson et al., 2016). In this regard, the minimum surface and envelope of morphodynamic change (Fig. 3b, c) provide valuable metrics for planning.

Ebb-tidal deltas are often perilous for navigation and frequently lead to shipwrecks (McNinch et al., 2001, 2006; Wells and McNinch, 2003; Torres, 2015). Knowledge of the maximum historic surface and envelope of morphodynamic change are thus valuable for safe navigation, since they indicate the shallowest and most dynamic regions of the ETD. In the event of a shipwreck or other such maritime incident, the stratigraphic modelling approach demonstrated here is also valuable for marine archaeology and salvage operations (e.g., the buried measurement frame in Fig. 5 F-F'). Our techniques are useful for any application where it is necessary to understand the burial and re-emergence of objects and infrastructure on ETDs.

5.4. Comparison with geological models

ETD stratigraphy has been well-explored and classified in previous studies, so here we present a comparison with our own technique. Imperato et al. (1988) and FitzGerald et al. (2012) identify three main elements of ebb-tidal delta architecture at mixed-energy tidal inlets:

1. *Marginal flood channel deposits*, characterized by steep, sharp erosional contact with adjacent barrier sand and upper shoreface deposits (e.g., Fig. 5 cross sections A-A', E-E'), as well as infilled channels topped by swash bar deposits. Imperato et al. (1988) notes that the shoreward migration of swash bars usually reworks deposits from previous bars, so that the complete sequence of a single bar is seldom preserved. This reflects what we see on the Bornrif: thin layers sediment gliding over the underlying platform without substantial vertical accretion.
2. *Proximal delta deposits* formed primarily by migration of the main ebb channel, thick and with a sharp contact with underlying Pleistocene sediment. Ameland Inlet is underlain by a highly resistant Pleistocene potclay layer between approximately –25 and –30 m NAP (van

- der Spek, 1994). This layer restricts the inlet channel depth and thus leads to a thinner inlet sequence compared to what would be expected in a completely sandy case. The thickest parts of the active delta are along the margins and bed of the former and current main ebb-channels (Fig. 3d). This is consistent with Moslow and Tye (1985), Imperato et al. (1988), and Sha (1989) who note that ebb-channel deposits tend to be the thickest, most preservable ETD facies on longer timescales. The repeating sigmoidal downdrift-dipping surfaces observed in Cross-Section F-F' (Fig. 5) are consistent with migrating inlet/spit systems (FitzGerald et al., 2012).
3. *Distal delta deposits*, which are 1–4 m thick and interweave with seaward shoreface sediment. These are evident in Cross Sections O-B', O-C', and G-G' (Fig. 5), and have been confirmed with vibrocoring samples offshore of the present study area by van der Spek et al. (2021).

Our results thus provide a clear explanation of the layering and sedimentary structures that are typically observed in the geological record. Previous studies mentioned above have largely relied on core samples, numerical models, and sparse surveys to construct stratigraphic models of ebb-tidal deltas, but the approach presented here provides a new way to find this information, and provides a novel perspective on the genesis of these architectural features. Future research should also consider relating the stratigraphy developed with this approach to observations of bed sediment particle size (e.g., Elias et al. (2022)).

5.5. Outlook

Having demonstrated our approach for Ameland ebb-tidal delta, the logical next steps for future research are to apply and extend these techniques at other tidal inlet systems. For instance, future studies could investigate more advanced techniques for optimizing the choice of origin (see also Supplementary material) or even use a conformal mapping layout that better reflects a given site's morphology than a fixed polar grid. Further developing such techniques may also enable automated analysis of e.g., global datasets of remote sensing-derived bathymetry. Ameland is a somewhat ideal case in that like many stabilized tide-dominated inlets (FitzGerald, 1984; Sha and De Boer, 1991; Tye and Moslow, 1993; Smith and FitzGerald, 1994; Elias et al., 2006; Son et al., 2011; Eelkema et al., 2013), it pivots around its inlet, so its dynamics map remarkably well to a polar grid. However, a polar coordinate system may not be the best choice for analyzing all ETDs, particularly multi-inlet systems or less stable wave-dominated inlets that migrate rapidly or close intermittently (Morales et al., 2001; Nienhuis and Ashton, 2016). Our method for developing a stratigraphic model from bathymetric surveys is applicable regardless of a system's dynamics, though. The main requirement is sufficiently high temporal resolution to capture the true reworking of sediment (Vonhögen-Peeters et al., 2013). For shallower ETDs, the necessary frequency of measurement could be obtained via remote sensing (e.g., Pianca et al. (2014); Harrison et al. (2017); Ford and Dickson (2018); Humberston et al. (2019); Zhang et al. (2020); Heimhuber et al. (2021)). Together, polar and stratigraphic analyses give researchers new means of simplifying and quantifying ETD dynamics, which could be used to quantitatively generalize ETD behaviour by examining other sites.

Although the temporal resolution of the Ameland dataset is high enough to resolve most decadal-scale morphodynamic changes, it is not sufficient to resolve seasonal patterns or the influence of specific storm events. To shed more light on these matters, the stratigraphic modelling approach could be further extended to process-based numerical model output. There are still many unresolved challenges in morphodynamic modelling of ebb-tidal deltas (Elias et al., 2015; Lenstra et al., 2019), and the results of this study can help in their analysis and interpretation by providing new types of information to validate against. Numerical models could also conceptually extend the present approach to look at

the role of grain size, sorting, and provenance in depositional processes, similarly to van der Vegt et al. (2020).

The approach demonstrated here is also likely to be applicable on other diverging sedimentary systems, such as alluvial fans, submarine fans, river-dominated deltas, or fan deltas. Distributary channels in these systems tend to radiate from a single outlet, which suggests that a radial collapse of the data could be an effective way to represent major morphodynamic trends.

6. Conclusions

We demonstrated the development and application of new approaches to mapping and analyzing ebb-tidal delta (ETD) dynamics, using the high resolution, frequent bathymetric surveys of Ameland Inlet in the Netherlands. Conformal mapping (polar) analysis provides a novel perspective on the analysis of ETD bypassing, by aligning the coordinates of analysis with the principle directions of sediment transport and morphodynamic evolution. In doing so, we transform the complex geometry of the ETD into a more convenient format for analyzing the morphologic patterns and sediment transport pathways that are of interest to coastal scientists and managers. With this approach, the bypassing behaviour described by Elias et al. (2019) and Elias et al. (2022) can be collapsed into fewer dimensions and the patterns expressed more simply as a timestamp. This enables the concept of ETD shoal bypassing and the rotational migration of ebb-tidal deltas to be investigated more continuously and quantitatively than previous efforts on the topic. There is a clear clockwise motion of shoals and channels of approximately 11°/decade, which corresponds to the dominant direction of longshore drift and offshore tidal dominance.

The interpretation made from the polar analysis is complemented by a decadal-scale stratigraphic model of Ameland ETD that we produced from the differences between repeated bathymetric surveys from 1975 to 2021. This approach permits the detailed analysis of deposit thickness, spatial distribution, age, and preservation potential. The majority of shoals in the active part of the ETD are continuously reworked on timescales of less than 10 years. These findings provide insight into the most stable regions of the ebb-tidal delta, which is important information for predicting how these features are likely to evolve in the future. This also provides a new and valuable approach for interpreting modern and ancient ETD stratigraphy.

Our analyses are permitted by the wealth of frequent, high-resolution bathymetric surveys conducted at Ameland Inlet. This method can be applied to any coastal system, but is best used where the data spans the dominant timescale of morphological change for the site, and with sufficiently high resolution in space and time to capture detailed phenomena. As such, the approach can also be applied to numerical model output. Together, the techniques presented here give researchers a new means of simplifying and quantifying ETD dynamics, and can lead to more generalized depictions of ETD behaviour. Furthermore, the approach can be applied to validate and interpret outcomes from numerical models. The improved understanding and practical techniques provide coastal managers with useful tools for sediment management and optimizing nourishment strategies in such complex environments. This will better prepare them to tackle future challenges posed by climate change and human interventions.

Declaration of competing interest

The authors declare that they have no known competing financial interests or personal relationships that could have appeared to influence the work reported in this paper.

Acknowledgements

This work is part of the research programme 'Collaboration Program Water' with project number 14489 (SEAWAD), which is (partly)

financed by NWO Domain Applied and Engineering Sciences. Special thanks to the Dutch Ministry of Infrastructure and Water Management (Rijkswaterstaat and Rijksrederij) for their ongoing support as part of the Kustgenese2.0 project. A special thank you is extended to Anna-Maartje de Boer who originally asked, “where is the oldest sand on the ebb-tidal delta?”, the question that inspired this analysis. We thank David Hoyal and an anonymous reviewer for their positive and constructive feedback. The *Vaklodingen* bathymetric data used in this study are publicly available at: <https://waterinfo-extra.rws.nl/monitoring/morfologie/>. *Actueel Hoogtebestand Nederland* (AHN) topographic data are available at <https://www.ahn.nl/>.

Appendix A. Supplementary data

Supplementary data to this article can be found online at <https://doi.org/10.1016/j.geomorph.2022.108185>.

References

- Brakenhoff, L., Ruessink, G., van der Vegt, M., 2019. Characteristics of saw-tooth bars on the ebb-tidal deltas of the Wadden Islands. *Ocean Dyn.* <https://doi.org/10.1007/s10236-019-01315-w>.
- Bridge, J.S., 1993. The interaction between channel geometry, water flow, sediment transport and deposition in braided rivers. In: Best, J.L., Bristow, C.S. (Eds.), *Braided Rivers*, pp. 13–71. Number 75.
- Cheung, K.F., Gerritsen, F., Cleveringa, J., 2007. Morphodynamics and sand bypassing at Ameland Inlet, the Netherlands. *J. Coast. Res.* 231, 106–118. <https://doi.org/10.2112/04-0403.1>.
- Duran-Matute, M., Gerken, T., Sassi, M.G., 2016. Quantifying the residual volume transport through a multiple-inlet system in response to wind forcing: the case of the western Dutch Wadden Sea. *J. Geophys. Res. Oceans* 121 (12), 8888–8903. <https://doi.org/10.1002/2016JC011807>.
- Eelkema, M., Wang, Z.B., Hibma, A., Stive, M.J., 2013. Morphological effects of the eastern scheldt storm surge barrier on the ebb-tidal delta. *Coast. Eng. J.* 55 (03), 1350010. <https://doi.org/10.1142/S0578563413500101>.
- Eelkema, M., Wang, Z.B., Stive, M.J., 2012. Impact of backbarrier dams on the development of the ebb-tidal delta of the Eastern Scheldt. *J. Coast. Res.* 28 (6), 1591–1605. <https://doi.org/10.2112/JCOASTRES-D-11-00003.1>. URL: <http://www.scopus.com/inward/record.url?eid=2-s2.0-84870160429%7B%7Dpartne> rID=40%7B%7Dmd5=9db177394b5f8717c5a072132d3e47ef%7B%25%7D5Cn.
- Eide, A., Malherbe, B., Mercanti, M., Lahousse, B., 1992. Assessment of coastal processes for the design and the construction of the Zeepipe landfall in Zeebrugge. In: *Coastal Engineering 1992*. American Society of Civil Engineers, Venice, Italy, pp. 1565–1569. <https://doi.org/10.1016/B978-0-323-04579-7.00156-8>.
- Elias, E.P.L., Pearson, S.G., van der Spek, A.J.F., Pluis, S., 2022. Understanding meso-scale processes at a mixed-energy tidal inlet: Ameland Inlet, the Netherlands – Implications for coastal maintenance. *Ocean Coast. Manag.* <https://doi.org/10.1016/j.ocecoaman.2022.106125>. In press.
- Elias, E.P., Cleveringa, J., Buijsman, M.C., Roelvink, J.A., Stive, M.J., 2006. Field and model data analysis of sand transport patterns in Texel Tidal inlet (the Netherlands). *Coastal Engineering* 53 (5–6), 505–529. <https://doi.org/10.1016/j.coastaleng.2005.11.006>. URL: <http://linkinghub.elsevier.com/retrieve/pii/S0378383905001729>.
- Elias, E.P., van der Spek, A.J.F., Lazar, M., 2015. The ‘Voordelta’, the contiguous ebb-tidal deltas in the SW Netherlands; Large-scale morphological changes and sediment budget 1965–2013; Impacts of large-scale engineering. *Neth. J. Geosci.* (November) <https://doi.org/10.1017/njg.2016.37>.
- Elias, E.P., van der Spek, A.J.F., Wang, Z.B., De Ronde, J., 2012. Morphodynamic development and sediment budget of the Dutch Wadden Sea over the last century. *Geol. Mijnb.* 91 (3), 293–310. <https://doi.org/10.1017/S001677460000457>.
- Elias, E.P., Van Der Spek, A.J.F., Pearson, S.G., Cleveringa, J., 2019. Understanding sediment bypassing processes through analysis of high- frequency observations of Ameland Inlet, the Netherlands. *Mar. Geol.* 415 (May), 105956 <https://doi.org/10.1016/j.margeo.2019.06.001>.
- FitzGerald, D.M., 1983. Sediment bypassing at mixed energy Tidal Inlets. *Proc. Coast. Eng. Conf.* 2, 1094–1118. <https://doi.org/10.9753/icce.v18.68>.
- FitzGerald, D.M., 1984. Interactions between the ebb-tidal delta and landward shoreline; Price Inlet, South Carolina. *J. Sediment. Res.* 54 (4), 1303–1318. <https://doi.org/10.1306/212F85C6-2B24-11D7-8648000102C1865D>. URL: <http://jssedres.sepmonline.org/content/54/4/1303.abstract>.
- FitzGerald, D.M., Buynevich, I., Hein, C., 2012. Morphodynamics and facies architecture of tidal inlets and tidal deltas. In: Davis, R.A., Dalrymple, R.W. (Eds.), *Principles of Tidal Sedimentology*. Springer Netherlands, Dordrecht, pp. 301–333. <https://doi.org/10.1007/978-94-007-0123-6> arXiv:arXiv:1011.1669v3.
- Fontolan, G., Pillon, S., Delli Quadri, F., Bezzi, A., 2007. Sediment storage at tidal inlets in northern Adriatic lagoons: Ebb-tidal delta morphodynamics, conservation and sand use strategies. *Estuar. Coast. Shelf Sci.* 75 (1–2), 261–277. <https://doi.org/10.1016/j.ecss.2007.02.029>.
- Ford, M.R., Dickson, M.E., 2018. Detecting ebb-tidal delta migration using Landsat imagery. *Mar. Geol.* 405 (December 2017), 38–46. <https://doi.org/10.1016/j.margeo.2018.08.002>.
- Fortunato, A., Freire, P., Mengual, B., Bertin, X., Pinto, C., Martins, K., Guérin, T., Azevedo, A., 2021. Sediment dynamics and morphological evolution in the Tagus Estuary inlet. *Mar. Geol.* 406. <https://doi.org/10.1016/j.scitotenv.2019.135601> doi:10.1016/j.margeo.2021.106590. URL: <https://linkinghub.elsevier.com/retrieve/pii/S0025322721001729>.
- Fruergaard, M., Pejrup, M., Murray, A.S., Andersen, T.J., 2015. On luminescence bleaching of tidal channel sediments. *Geografisk Tidsskrift - Danish J. Geogr.* 115 (1), 57–65. <https://doi.org/10.1080/00167223.2015.1011418>.
- Gelfenbaum, G., Kaminsky, G.M., 2010. Large-scale coastal change in the Columbia River littoral cell: an overview. *Mar. Geol.* 273 (1–4), 1–10. <https://doi.org/10.1016/j.margeo.2010.02.007>.
- Harrison, S.R., Bryan, K.R., Mularney, J.C., 2017. Observations of morphological change at an ebb-tidal delta. *Marine Geology* 385, 131–145. <https://doi.org/10.1016/j.margeo.2016.12.010>. URL: <http://linkinghub.elsevier.com/retrieve/pii/S0025322716303929> URL: <https://linkinghub.elsevier.com/retrieve/pii/S0025322716303929>.
- Hayes, M.O., 1980. General morphology and sediment patterns in tidal inlets. *Sediment. Geol.* 20 (1–3), 139–156. [https://doi.org/10.1016/0037-0738\(80\)90009-3](https://doi.org/10.1016/0037-0738(80)90009-3).
- Heimhuber, V., Vos, K., Fu, W., Glamore, W., 2021. InletTracker: an open-source Python toolkit for historic and near real-time monitoring of coastal inlets from Landsat and Sentinel-2. *Geomorphology* 389, 107830. <https://doi.org/10.1016/j.geomorph.2021.107830>.
- Herrling, G., Winter, C., 2018. Tidal inlet sediment bypassing at mixedenergy barrier islands. *Coast. Eng.* 140 (October 2017), 342–354. <https://doi.org/10.1016/j.coastaleng.2018.08.008>. URL: <http://linkinghub.elsevier.com/retrieve/pii/S0378383919305896>.
- Hicks, D.M., Hume, T.M., 1997. Determining sand volumes and bathymetric change on an ebb-tidal delta. *J. Coast. Res.* 13 (2), 407–416.
- Hovmøller, E., 1949. The Trough-and-Ridge diagram. *Tellus* 1 (2), 62–66.
- Hubbard, D., Oertel, G., Nummedal, D., 1979. The role of waves and tidal currents in the development of tidal-inlet sedimentary structures and sand body geometry: examples from North Carolina, South Carolina, and Georgia. *J. Sediment. Petrol.* 49 (4), 1073–1092.
- Humberston, J., Lippmann, T., McNinch, J., 2019. Observations of wave influence on alongshore ebb-tidal delta morphodynamics at Oregon Inlet, NC. *Marine Geology* 418 (December), 106040. <https://doi.org/10.1016/j.margeo.2019.106040>. URL: <https://linkinghub.elsevier.com/retrieve/pii/S0025322718304377>.
- Imperato, D.P., Sexton, W.J., Hayes, M.O., 1988. Stratigraphy and sediment characteristics of a mesotidal ebb-tidal delta, North Edisto Inlet, South Carolina. *J. Sediment. Res.* 58 (6), 950–958. <https://doi.org/10.1306/212F8EC7-2B24-11D7-8648000102C1865D>.
- Israel, C.G., Dunsbergen, D.W., 1999. Cyclic morphological development of the Ameland Inlet, the Netherlands. In: *Proceedings of Symposium on River, Coastal and Estuarine Morphodynamics*. Genova, Italy, pp. 705–714.
- Jerolmack, D.J., Paola, C., 2010. Shredding of environmental signals by sediment transport. *Geophys. Res. Lett.* 37 (19), 1–5. <https://doi.org/10.1029/2010GL044638>.
- Kaminsky, G.M., Ruggiero, P., Buijsman, M.C., McCandless, D., Gelfenbaum, G., 2010. Historical evolution of the Columbia River littoral cell. *Mar. Geol.* 273 (1–4), 96–126. <https://doi.org/10.1016/j.margeo.2010.02.006>.
- Kana, T.W., Hayter, E.J., Work, P.A., 1999. Mesoscale sediment transport at southeastern U.S. tidal inlets: conceptual model applicable to mixed energy settings. *J. Coast. Res.* 15 (2), 303–313.
- Kleinhan, M.G., 2010. Sorting out river channel patterns. *Prog. Phys. Geogr.* 34 (3), 287–326. <https://doi.org/10.1177/0309133310365300>.
- Lambregts, P., 2021. Understanding Sediment Bypassing at Ameland Inlet. Delft University of Technology. Msc thesis.
- Lazarus, E.D., Harley, M.D., Blenkinsopp, C.E., Turner, I.L., 2019. Environmental signal shredding on sandy coastlines. *Earth Surface Dynamics* 7 (1), 77–86. <https://doi.org/10.5194/esurf-7-77-2019>.
- Lenstra, K.J., Pluis, S.R., Ridderinkhof, W., Ruessink, G., van der Vegt, M., 2019. Cyclic channel-shoal dynamics at the Ameland inlet: the impact on waves, tides, and sediment transport. *Ocean Dyn.* 69 (4), 409–425. <https://doi.org/10.1007/s10236-019-01249-3>.
- Lodder, Q., Slinger, J.H., 2021. The ‘Research for Policy’ cycle in Dutch coastal flood risk management: the Coastal Genesis 2 research programme. *Ocean Coast. Manag.* 219, 106066 <https://doi.org/10.1016/j.ocecoaman.2022.106066>.
- Lodder, Q.J., Wang, Z.B., Elias, E.P., van der Spek, A.J., de Looff, H., Townsend, I.H., 2019. Future response of the Wadden Sea tidal basins to relative sea-level rise—an aggregated modelling approach. *Water* 11 (10). <https://doi.org/10.3390/w11102198>.
- MacDonald, N.J., Davies, M.H., 2007. Particle-based sediment transport modelling. In: *Coastal Engineering 2006*, 3. World Scientific Publishing Company, pp. 3117–3128.
- McNinch, J.E., Wells, J.T., Drake, T.G., 2001. The fate of artifacts in an energetic, shallow-water environment: scour and burial at the wreck site of Queen Anne’s revenge. *Southeast. Geol.* 40 (1), 19–27.
- McNinch, J.E., Wells, J.T., Trembanis, A.C., 2006. Predicting the fate of artefacts in energetic, shallow marine environments: an approach to site management. *Int. J. Naut. Archaeol.* 35 (2), 290–309. <https://doi.org/10.1111/j.1095-9270.2006.00105.x>.
- Morales, J.A., Borrego, J., Jiménez, I., Monterde, J., Gil, N., 2001. Morphostratigraphy of an ebb-tidal delta system associated with a large spit in the Piedras Estuary mouth (Huelva Coast, Southwestern Spain). *Mar. Geol.* 172 (3–4), 225–241. [https://doi.org/10.1016/S0025-3227\(00\)00135-3](https://doi.org/10.1016/S0025-3227(00)00135-3).

- Moslow, T.F., Tye, R.S., 1985. Recognition and characterization of Holocene tidal inlet sequences. *Mar. Geol.* 63 (1–4), 129–151. [https://doi.org/10.1016/0025-3227\(85\)90081-7](https://doi.org/10.1016/0025-3227(85)90081-7).
- Mulhern, J.S., Johnson, C.L., Green, A.N., 2021. When is a barrier island not an island? When it is preserved in the rock record. *Frontiers in Earth Science* 8 (February). <https://doi.org/10.3389/feart.2020.560437>. <https://www.frontiersin.org/articles/10.3389/feart.2020.560437/full>.
- Nicholas, A.P., Sambrook Smith, G.H., Amsler, M.L., Ashworth, P.J., Best, J.L., Hardy, R.J., Lane, S.N., Orfeo, O., Parsons, D.R., Reesink, A.J., Sandbach, S.D., Simpson, C.J., Szupiany, R.N., 2016. The role of discharge variability in determining alluvial stratigraphy. *Geology* 44 (1), 3–6. <https://doi.org/10.1130/G37215.1>.
- Nienhuis, J.H., Ashton, A.D., 2016. Mechanics and rates of tidal inlet migration: Modeling and application to natural examples. *Journal of Geophysical Research: Earth Surface* 121 (11), 2118–2139. <https://doi.org/10.1002/2016JF004035>.
- Oost, A.P., Hoekstra, P., Wiersma, A., Flemming, B.W., Lammerink, E.J., Pejrup, M., Hofstede, J., van der Valk, B., Kiden, P., Bartholdy, J., van der Berg, M.W., Vos, P.C., de Vries, S., Wang, Z.B., 2012. Barrier island management: Lessons from the past and directions for the future, 68, 18–38. <https://doi.org/10.1016/j.ocecoaman.2012.07.010>.
- Parker, G., Sequeiros, O., 2006. Large scale river morphodynamics: application to the Mississippi Delta. In: *Proceedings of the International Conference on Fluvial Hydraulics - River Flow 2006*, 1, pp. 3–11.
- Pearson, S.G., Elias, E., van Ormondt, M., Roelvink, F., Lambregts, P., Wang, Z., van Prooijen, B.C., 2021. Lagrangian sediment transport modelling as a tool for investigating coastal connectivity. In: *Coastal Dynamics 2021*. Delft, The Netherlands.
- Pearson, S.G., Lubbad, R., Le, T.M., Baird, R.B., 2016. Thermomechanical erosion modelling of Baydaratskaya Bay, Russia with COSMOS. In: *Scour and Erosion - Proceedings of the 8th International Conference on Scour and Erosion, ICSE 2016*, pp. 281–291. <https://doi.org/10.1201/9781315375045-34>.
- Pearson, S.G., van Prooijen, B.C., Elias, E.P.L., Vitousek, S., Wang, Z.B., 2020. Sediment connectivity: a framework for analyzing coastal sediment transport pathways. *J. Geophys. Res. Earth Surf.* 125 (10) <https://doi.org/10.1029/2020JF005595>. <https://onlinelibrary.wiley.com/doi/10.1029/2020JF005595>.
- Pearson, S.G., van Prooijen, B.C., Poleykett, J., Wright, M., Black, K., Wang, Z.B., 2021. Tracking fluorescent and ferrimagnetic sediment tracers on an energetic ebb-tidal delta to monitor grain size-selective dispersal. *Ocean & Coastal Management* 212, 105835. <https://doi.org/10.1016/j.ocecoaman.2021.105835>. <https://linkinghub.elsevier.com/retrieve/pii/S0964569121003185>.
- Pearson, S.G., van Prooijen, B.C., de Wit, F.P., Meijer-Holzhauer, H., de Looff, A., Wang, Z.B., 2019. Observations of suspended particle size distribution on an energetic ebb-tidal delta. *Coast. Sediments* 2019, 1991–2003. https://doi.org/10.1142/9789811204487_0172.
- Pianca, C., Holman, R., Siegle, E., 2014. Mobility of meso-scale morphology on a microtidal ebb delta measured using remote sensing. *Mar. Geol.* 357, 334–343. <https://doi.org/10.1016/j.margeo.2014.09.045>.
- Power, H.E., Pomeroy, A.W.M., Kinsela, M.A., Murray, T.P., 2021. Research priorities for coastal geoscience and engineering: a collaborative exercise in priority setting from Australia. *Front. Mar. Sci.* 8 (April) <https://doi.org/10.3389/fmars.2021.645797>.
- van Prooijen, B.C., Tissier, M., de Wit, F.P., Pearson, S.G., Brakenhoff, L., van Maarseveen, M., van der Vegt, M., Mol, J.W., Kok, F., Holzhauer, H., van der Werf, J., Vermaas, T., Gaweijn, M., Grasmeijer, B., Elias, E.P., Tonnon, P.K., Reniers, A., Wang, Z.B., den Heijer, C., van Gelder-Maas, C., Wilmink, R., Schipper, C., de Looff, H., 2020. Measurements of hydrodynamics, sediment, morphology and benthos on Ameland ebb-tidal delta and lower shoreface. *Earth Syst. Sci. Data* 2 (November), 1–18. <https://doi.org/10.5194/essd-2020-13>.
- Reimann, T., Notenboom, P.D., de Schipper, M.A., Wallinga, J., 2015. Testing for sufficient signal resetting during sediment transport using a polymimetic multiple-signal luminescence approach. *Quat. Geochronol.* 25, 26–36. <https://doi.org/10.1016/j.quageo.2014.09.002>.
- Ridderinkhof, W., Hoekstra, P., Van Der Vegt, M., de Swart, H.E., 2016. Cyclic behavior of sandy shoals on the ebb-tidal deltas of the Wadden Sea. *Cont. Shelf Res.* 115, 14–26. <https://doi.org/10.1016/j.csr.2015.12.014>.
- Rijkswaterstaat, Waddenze, Sedimentatlas, 1999. Haren, Netherlands: Rijkswaterstaat. <https://publicwiki.deltares.nl/display/OET/Dataset+documentation+Sediment+atlas+wadden+sea>.
- Ronchi, L., Fontana, A., Correggiari, A., Remia, A., 2019. Anatomy of a transgressive tidal inlet reconstructed through high-resolution seismic profiling. *Geomorphology* 343, 65–80. <https://doi.org/10.1016/j.geomorph.2019.06.026>.
- Rosati, J.D., 2005. Concepts in sediment budgets. *J. Coast. Res.* 21 (2), 307–322. <https://doi.org/10.2112/02-475A.1>.
- Schinzinger, R., Laura, P.A.A., 2003. *Conformal Mapping: Methods and Applications*. Dover Publications, Mineola, New York.
- Sha, L.P., 1989. Holocene-Pleistocene interface and three-dimensional geometry of the ebb-delta complex, Texel Inlet, The Netherlands. *Marine Geology* 89 (3–4), 207–228. [https://doi.org/10.1016/0025-3227\(89\)90076-5](https://doi.org/10.1016/0025-3227(89)90076-5).
- Sha, L.P., De Boer, P.L., 1991. Ebb-tidal delta deposits along the west Frisian Islands (the Netherlands): processes, facies architecture and preservation. *Clastic Tidal Sedimentol.* 16 (1991), 199–218. URL: <http://www.scopus.com/inward/record.url?eid=2-s2.0-0026395606&partnerID=40&md5=6d1168385f3d00b4e587ad3a5a4fcafb>.
- Smith, J.B., Fitzgerald, D.M., 1994. Sediment transport patterns at the Essex River Inlet ebb-tidal delta, Massachusetts, U.S.A. *J. Coast. Res.* 10 (3), 752–774.
- Son, C.S., Flemming, B.W., Bartholoma, A., 2011. Evidence for sediment recirculation on an ebb-tidal delta of the East Frisian barrier-island system, southern North Sea. *Geol. Mar. Lett.* 31 (2), 87–100. <https://doi.org/10.1007/s00367-010-0217-8>.
- Soulsby, R.L., Mead, C.T., Wild, B.R., Wood, M.J., 2011. Lagrangian model for simulating the dispersal of sand-sized particles in coastal waters. *J. Waterw. Port Coast. Ocean Eng.* 137 (3), 123–131. [https://doi.org/10.1061/\(ASCE\)WW.1943-5460.000074](https://doi.org/10.1061/(ASCE)WW.1943-5460.000074).
- van der Spek, A.J., Forzani, A., Vermaas, T., 2021. Geology of the Dutch lower shoreface. Submitted to: *Ocean Coast. Manag.* 1–26.
- van der Spek, A.J.F., 1994. *Large-scale Evolution of Holocene Tidal Basins in the Netherlands*. Utrecht University. Phd.
- van der Spek, A.J.F., 1996. Holocene depositional sequences in the Dutch Wadden Sea south of the island of Ameland. *Med. Rijks Geol. Dienst.* 57, 41–78.
- Stive, M.J., Wang, Z.B., 2003. Morphodynamic modeling of tidal basins and coastal inlets. In: *Elsevier Oceanography Series*, 67, pp. 367–392. [https://doi.org/10.1016/S0422-9894\(03\)80130-7](https://doi.org/10.1016/S0422-9894(03)80130-7).
- Straub, K.M., Duller, R.A., Foreman, B.Z., Hajek, E.A., 2020. Buffered, incomplete, and shredded: the challenges of reading an imperfect stratigraphic record. *J. Geophys. Res. Earth Surf.* 125 (3), 1–44. <https://doi.org/10.1029/2019JF005079>.
- Sylvester, Z., Pirmez, C., Cantelli, A., 2011. A model of submarine channel levee evolution based on channel trajectories: implications for stratigraphic architecture. *Mar. Pet. Geol.* 28 (3), 716–727. <https://doi.org/10.1016/j.marpetgeo.2010.05.012>.
- Torres, R.D.O., 2015. *The Archaeology of Shore Stranded Shipwrecks of Southern Brazil*. Texas A&M University. Ph.D. thesis.
- Tye, R.S., Moslow, T.F., 1993. In: *Tidal Inlet Reservoirs: Insights From Modern Examples*, pp. 77–99. https://doi.org/10.1007/978-1-4757-0160-9_4 (C).
- Van Weerdenburg, R.J., Pearson, S.G., van Prooijen, B.C., Laan, S., Elias, E., 2021. Field measurements and numerical modelling of wind-driven exchange ows in a tidal inlet system in the Dutch Wadden Sea. *Ocean Coast. Manag.* 215 (October), 105941. <https://doi.org/10.1016/j.ocecoaman.2021.105941>.
- van der Vegt, H., 2018. From Uvial Supply to Delta Deposits: Simulating Sediment Delivery, Transport and Deposition. Phd. Delft University of Technology. <https://doi.org/10.4233/uuid:c049ea67-23a1-4e7eaf52-1275802839f1>.
- van der Vegt, H., Storms, J.E., Walstra, D.R., Nordahl, K., Howes, N.C., Martinus, A.W., 2020. Grain size fractionation by process-driven sorting in sandy to muddy deltas. *Depositional Rec.* 6 (1), 217–235. <https://doi.org/10.1002/dep2.85>. <https://onlinelibrary.wiley.com/doi/abs/10.1002/dep2.85>.
- Vonhögen-Peeters, L.M., van Heteren, S., Wiersma, A.P., de Kleine, M.P., Marges, V.C., 2013. Quantifying sediment dynamics within the Dutch Wadden Sea using bathymetric monitoring series. *J. Coast. Res.* 165 (65), 1611–1616. <https://doi.org/10.2112/si65-272.1>.
- Walton, T.L., Adams, W.D., 1976. In: *Capacity of Inlet Outer Bars to Store Sand*. 15th Coastal Engineering Conference, pp. 1919–1937. <https://doi.org/10.9753/icce.v15>.
- Wang, Z.B., Townsend, I., Stive, M.J., 2020. Aggregated morphodynamic modeling of tidal inlets and estuaries. *Water Sci. Eng.* 13 (1), 1–13. <https://doi.org/10.1016/j.wse.2020.03.004>.
- Wells, J.T., McNinch, J.E., 2003. Role of inlet dynamics in scour and burial of marine artifacts in energetic coastal settings. In: *WIT Transactions on the Built Environment*, 65, pp. 87–96.
- van der Werf, J., Antolínez, J.A.Á., Brakenhoff, L., Gaweijn, M., den Heijer, K., de Looff, H., Wilmink, R., van Maarsseveen, M., Meijer-Holzhauer, H., Mol, J.W., Pearson, S.G., van Prooijen, B.C., Santinelli, G., Schipper, C., Tissier, M., Tonnon, P.K., de Vet, L., Vermaas, T., Wilmink, R.J., de Wit, F.P., 2019. *Datareport Kustgenese 2.0. Technical Report 1220339-015-ZKS-0004; Rijkswaterstaat*; Delft, The Netherlands.
- Zhang, H., Li, D., Wang, J., Zhou, H., Guan, W., Lou, X., Cao, W., Shi, A., Chen, P., Fan, K., Ren, L., Zheng, G., Li, Y., 2020. Long time-series remote sensing analysis of the periodic cycle evolution of the inlets and ebb-tidal delta of Xincun Lagoon, Hainan Island, China. *ISPRS J. Photogramm. Remote Sens.* 165 (February), 67–85. <https://doi.org/10.1016/j.isprsjprs.2020.05.006>.
- Zhu, H., Zuo, L., Lu, Y., 2019. Process-based modeling on morphology evolution of Laolonggou Tidal Inlet in Bohai Bay of China. In: *Coastal Sediments 2019. World Scientific*, St. Petersburg, Florida, pp. 2057–2079.
- Zijderveld, A., Peters, H., 2009. Measurement programme Dutch Wadden Sea. In: *Coastal Engineering 2008. World Scientific*, Hamburg, Germany, pp. 404–410.